*Transactions*, **SMiRT-22**
**San Francisco, California, USA - August 18-23, 2013**
**Division IX (include assigned division number from I to X)**

# IDENTIFICATION OF DUCTILE DAMAGE PARAMETERS FOR PRESSURE VESSEL STEEL

Jan Dzugan[1], Antonin Prantl[2], Miroslav Spaniel[3], Pavel Konopik[4], Jan Ruzicka[5] and Jiri Kuzelka[5]

[1]Head of department, Dept. of Mechanical Testing and Thermophysical measurements, COMTES FHT a.s., Dobrany, Czech Republic (jan.dzugan@comtesfht.cz)
[2]Senior research engineer, NPP services, SKODA JS a.s., Pilsen, Czech Republic
[3]Ass. Prof., Dept. of Mechanics, biomechanics and mechatronics, Czech Technical University, Prague, Czech Rep.
[4]Deputy head of dep., Dept. of Mechanical Testing Laboratory, COMTES FHT a.s., Dobrany, Czech Republic
[5]Ph.D. student, Dept. of Mechanics, biomechanics and mechatronics, CTU, Prague, Czech Republic

## ABSTRACT

The FEM simulations in the field of design and safety assessment represent very powerful tools, but they are strongly limited by available material models and material input data. Many of the current calculations are still performed on the basis of standard tensile tests, if not only on database data or data from literature. Such a material description is not sufficient for an accurate design assessment and detailed material behavior description has to be used for a reliable results.

Standard tensile test is mainly based on uniaxial sample loading and small strains. The standard tensile test results are useful for elastic solutions or elastic-plastic solution for a small plastic strains. If states near to fracture are to be considered, more complex material description taking into account multiaxial loading conditions is necessary; Bai (2008, 2010), Wierbitzski (2005), Bao (2004), Li (2009). Thus samples of various geometries tested under various loading modes have to be used. On the basis of these tests a complex material behavior model covering elastic and plastic material behavior for various triaxiality states can be obtained. This kind of the material behavior description allows a wide range of application from calculation of component limit loading conditions to material properties conversion for samples of different sizes e.g..

The Current paper is dealing with ductile damage parameters determination for two typical Reactor Pressure Vessel (RPV) steels ferritic and austenitic. The ferritic steel is used for the RPV vessel and the austenitic one is used for internals. There are chosen appropriate samples geometries based on the FEM stress state analyses of samples at first. Subsequently, testing of proposed samples is performed and material parameters are evaluated. The obtained material plastic damage parameters are subsequently applied to FEM simulation of sharp notched samples and capabilities of applied models to describe material behavior for high stress concentrations is assessed on the basis comparison with real tests.

## INTRODUCTION

Ductile damage is the process of metallic material damage under conditions of monotonic loading. Evolution of the damage follows plastic straining and ends by fracture of component. Problems of ductile damage play significant role in industry, for example in optimization of technological processes, evaluation of safety in automotive and aeronautic industry, analysis of steel civil structures etc. Complex material models of ductile fracture require calibration based on extensive experimental tests.

Phenomenological material models describing ductile damage in continuum mechanics mostly introduce extension of plasticity models. Two types of material models can be distinguished. Uncoupled models separate plastic response and ductile damage and failure. Coupled models modify plastic response in dependence on damage evolution. Even though coupled models have huge potential, their complexity

and calibration costs results into small extension in practice. Easier calibration process is an essential advantage of uncoupled material models, for which the calibration of plastic response and calibration of ductile damage can be separated. The calibration is significantly easier when the uncoupled material model is used.

In the current paper uncoupled material models using Johnson-Cook, Rice-Tracey and Bai-Wierbitzski damage description are applied to two steels: ferritic one and austenitic one used in RPV applications. The ductile damage parameters are determined for considered materials on the basis of experimental results and FEM simulations. The damage parameters are subsequently applied to simulation of notched fracture mechanics samples designed as CT (Central Tension). The results of simulation of CT samples are compared with the experimental results.

## DUCTILE DAMAGE MODEL

Material model discussed in this paper is based on both classical incremental model of plastic response with isotropic hardening and phenomenological concept of damage in continuum mechanic. This model supposes isotropy, and for description of stress state uses Von Mises stress $q$, stress triaxiality $\eta$ and Lode parameter $\xi$. These quantities are defined using second and third invariant of deviatoric stress according to Equation 1.

$$J_2 = \frac{1}{2}\left(S_1^2 + S_2^2 + S_3^2\right), \; J_3 = S_1 S_2 S_3 \qquad 1$$

Principal deviatoric stresses $S_1$, $S_2$ and $S_3$ are principal values of stress deviator, Equation 2.

$$\mathbf{S} = \boldsymbol{\sigma} + p\mathbf{I} \qquad 2$$

where

$$p = -\frac{1}{3} tr\left(\boldsymbol{\sigma}\right), \qquad 3$$

where $p$ is hydrostatic stress. Von Mises stress is defined in Equation 4:

$$q = \sqrt{3J_2} \; . \qquad 4$$

Stress triaxiality $\eta$ can be expressed by Equation 5

$$\eta = -\frac{p}{q} \qquad 5$$

Lode parameter $\xi$ can be expressed by following Equation 6

$$\xi = \frac{27}{2}\frac{J_3}{q} . \qquad 6$$

and the normalized Lode angle can be expressed according to Equation 7:

$$\bar{\theta} = \frac{6\theta}{\pi} = 1 - \frac{2}{\pi}\arccos\xi \qquad 7$$

The model of plastic response works with simple plane of plasticity that is based on Von Mises stress according to Equation 8.

$$q = \sigma_Y\left(\bar{\varepsilon}_{pl}\right) \qquad 8$$

associated flow rule and has the only one history dependent state parameter – accumulated intensity of plastic strain, resp. accumulated plastic strain, Equation 9.

$$\bar{\varepsilon}_{pl} = \int_0^t \dot{\bar{\varepsilon}}_{pl} dt \qquad 9$$

where

$$\dot{\bar{\varepsilon}}_{pl} = \sqrt{\frac{2}{3}\dot{\boldsymbol{\varepsilon}}_{\mathbf{pl}} : \dot{\boldsymbol{\varepsilon}}_{\mathbf{pl}}} \qquad 10$$

Relation of $\sigma_Y\left(\bar{\varepsilon}_{pl}\right)$ is calibrated experimentally.

Failure criterion is based on phenomenological quantity damage $\omega$, that is defined as non-decreasing scalar parameter, Equation 11

$$\omega = \int_0^t \frac{\dot{\bar{\varepsilon}}_{pl} dt}{\bar{\varepsilon}_f\left(\eta, \xi\right)} \qquad 11$$

that depends on loading history and can be understood as linear accumulation of incremental damage in process of monotonic loading. Fracture locus $\bar{\varepsilon}_f$ is function of stress triaxiality and Lode parameter and it has to be calibrated experimentally. Ductile fracture of material occurs as soon as critical damage value $\omega_{crit}$ is reached. The fracture locus has physical meaning of accumulated plastic strain at the instant of ductile damage initiation at the end of hypothetic monotonic loading with both triaxiality and Lode parameter constant. In such loading process the damage at failure reaches value $\omega_{crit} = 1$, so damage defined in Equation 11 can be said to be normalized.

In this paper Johnson-Cook and Rice Tracey material models were employed for description of ductile damage for ferritic steel and Bai-Wierzbicki and expanded Bai-Wierzbicki models were used for austenitic material.

Johnson cook model in following form was used, Equation 12:

$$\bar{\varepsilon}_f\left(\eta, \dot{\bar{\varepsilon}}_{pl}, \hat{T}\right) = \left[d_1 + d_2 e^{-d_3\eta}\right]\left[1 + d_4 \ln\left(\frac{\dot{\bar{\varepsilon}}_{pl}}{\dot{\varepsilon}_0}\right)\right]\left(1 + d_5\hat{T}\right) \qquad 12$$

where $d_1 \ldots d_5$ are failure parameters, $\dot{\varepsilon}_0$ is the reference strain rate, and $\hat{T}$ is the dimensionless temperature. In this paper quasi-static loading at room temperature is supposed. Therefore the first term (parameters $d_1, d_2, d_3$) of Johnson-Cook model is calibrated only.

Exponential dependence of fracture locus on stress triaxiality also appears in material model Rice-Tracey , Rice (1969) that is based on description of growing micro-cavities in basic material matrix. The Rice-Tracey model is defined by Equation 13:

$$\bar{\varepsilon}_f\left(\eta\right) = C_{RT} e^{-\frac{3}{2}\eta}, \qquad 13$$

where $C_{RT}$ is failure parameter that has to be calibrated.

The Bai-Wierzbicki material model, Bai (2008, 2010), is also employed to describe ductile damage. Xue and Wierzbicki (2005) expanded the dependence of the fracture strain on triaxiality by a third invariant of the stress tensor. This invariant was included in the form of the Lode parameter. Xue and Wierybicki used an elliptical function to describe the dependence of the fracture locus on the Lode parameter. They defined the fracture locus as a symmetric function that shows the same dependence of tension $\left(\bar{\theta} = 1\right)$,and pressure $\left(\bar{\theta} = -1\right)$ of notched round bars.

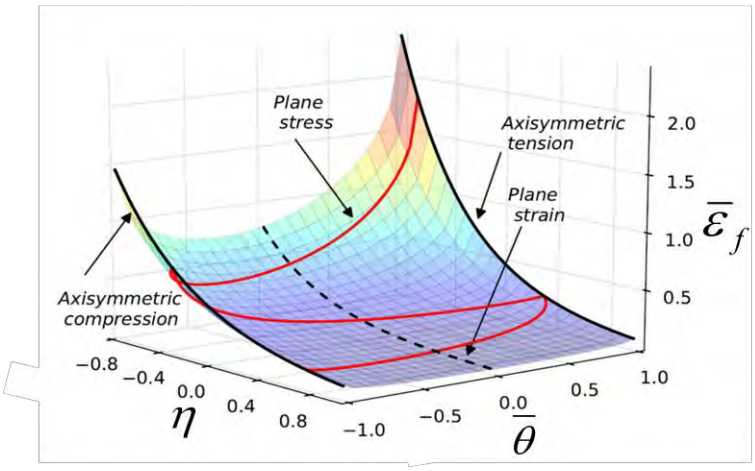


Figure 1. Asymmetric fracture locus.

A further generalization is introduced in the Bai-Wierzbicki model, Bai (2008) which expects the fracture locus to be generally asymmetric, Figure 1. The dependence of the fracture locus on the third invariant of the stress tensor introduced using the normalized Lode angle has the form of a parabolic function. The influence of stress triaxiality is described as an exponential form Equation 13. Fracture locus is expressed using round bar tension $(\bar{\theta}=1)$, plane strain $(\bar{\theta}=0)$ and round bar pressure $(\bar{\theta}=-1)$, Equation 14.

$$\bar{\varepsilon}_f(\eta,\bar{\theta}) = A_1(\eta)\bar{\theta}^2 + A_2(\eta)\bar{\theta} + A_3(\eta);\quad \begin{aligned} \bar{\varepsilon}_f(\eta,1) &= D_1 e^{-D_{2\eta}} \\ \bar{\varepsilon}_f(\eta,0) &= D_3 e^{-D_{4\eta}} \\ \bar{\varepsilon}_f(\eta,-1) &= D_5 e^{-D_{6\eta}} \end{aligned} \qquad 14$$

After some manipulations, the model can be expressed in final form of Equation 15

$$\bar{\varepsilon}_f(\eta,\bar{\theta}) = \frac{1}{2}\left[\left(D_1 e^{-D_{2\eta}} + D_5 e^{-D_{6\eta}}\right) - D_3 e^{-D_{4\eta}}\right]\bar{\theta}^2 + \frac{1}{2}\left(D_1 e^{-D_{2\eta}} - D_5 e^{-D_{6\eta}}\right)\bar{\theta} + D_3 e^{-D_{4\eta}} \qquad 15$$

The artificial degradation function described by parameter of degradation is implemented in Abaqus software and is implemented in order to prevent gradual loss of stiffness in the whole element at the instant when the failure criterion is reached. Difference between damage and degradation process is in relation to fracture strain. The degradation is not included as material parameter and therefore it is not included in calibration process. Nevertheless the results of numerical simulation can be affected by choice of degradation. Since failure is indicated in the element of FE mesh the degradation manifesting itself as decrease of elastic modulus is started as Equation 16.

$$E^* = (1-D)E \qquad 16$$

After the critical value $D=1$ is reached in element, it is removed form FE mesh. The damage process could be controlled by more ways in Abaqus. In this paper the description based on Hillerborg's fracture energy was used, Equation 17

$$G_f = \int \mathrm{q}\, du_{pl} = \int Lq\, d\bar{\varepsilon}_{pl} \qquad 17$$

Degradation process is defined as Equation 18

$$D = \int \frac{Lq}{G_f} d\bar{\varepsilon}_{pl} \qquad 18$$

where $L$ is characteristic size of element. As the Equation 18 shows, dependence of damage trend on characteristic size of element $L$ is disadvantage of this approach. In area of expected damage the mesh with the same element size should be used. Material parameter $G_f$ must be recalculated for different mesh density. From Equation 17 the fracture energy $G_f$ can be expressed for any characteristic element length $L$ differing from $L_0$ using values of $G_{f0}$, Equation 19.

$$\frac{G_f}{L} = \frac{G_{f0}}{L_0} = \int \mathrm{q}\, d\bar{\varepsilon}_{pl} \;\; , \; G_f = \frac{G_{f0}}{L_0} L \qquad 19$$

Dependency of degradation development on mesh density can be removed by setting $G_f \to 0$. The phase of degradation is minimized and the full degradation of element occurs immediately after the critical damage value $\omega_{crit}$ is reached. All samples simulated in this paper have the same size of element edge (0.2 mm) in expected damage initiation. Small punch is exception. The element size of this type of specimen is 0.05 mm.

## METHODS OF CALLIBRATION

Several specimen types with different values of both stress triaxiality and Lode parameter at expected locations of ductile fracture should be used for successful calibration of material model. Because in most cases the course of quantities ($\eta, \xi, \bar{\varepsilon}_{pl}$) during loading process can not be described using analytic formulas, the specimens have to be analyzed via FE. The calculated course of these quantities serves as input into calibration process. Experimental determination of fracture strain $\bar{\varepsilon}_f$ is essential. Mostly the critical extension $\Delta L_f$ at the instant of failure is determined from experimental data. Fracture strain $\bar{\varepsilon}_f$ in expected location of failure is then calculated using FE simulation. The critical extension could be determined for example via direct surface observation and first individual cracks detection. This approach is limited onto specimens at which the fracture starts form surface. Usually, critical extension is identified on base of sudden decrease of loading force in force-displacement record. It is possible to use the method of digital image correlation for direct evaluation of fracture strain in case of failure on the surface.

Two approaches are commonly cited to be used in calibration process of uncoupled ductile damage model. The first one is based on averaged values of stress triaxiality and Lode parameter, Bai (2007) etc. Averaged values of stress triaxiality $\eta_{av}$ are calculated according to following expression, Equation 20:

$$\eta_{av} = \frac{1}{\bar{\varepsilon}_f} \int_0^{\bar{\varepsilon}_f} \eta\left(\bar{\varepsilon}_{pl}\right) d\bar{\varepsilon}_{pl}, \qquad 20$$

Lode parameter weighted average $\xi_{av}$ is expressed as Equation 21

$$\text{resp.}\, \xi_{av} = \frac{1}{\bar{\varepsilon}_f} \int_0^{\bar{\varepsilon}_f} \xi\left(\bar{\varepsilon}_{pl}\right) d\bar{\varepsilon}_{pl} \qquad 21$$

The point $\left[\eta_{av}, \xi_{av}, \bar{\varepsilon}_f\right]$ for each individual sample can be determined by this approach. Fracture locus $\bar{\varepsilon}_f(\eta, \xi)$ passes through this point. The main disadvantage of this approach is wide range of stress triaxiality and Lode parameter $\xi$ for some specimen types resulting into non-negligible error caused by averaging of these quantities. The point of minimum of target functional $F_{av}$, Equation 22:

$$F_{av} = \frac{1}{N}\sum_{i=1}^{N}\left| \bar{\varepsilon}_{f_i} - \bar{\varepsilon}_f\left(\eta_{av_i}, \xi_{av_i}\right)\right|^m \qquad 22$$

is searched employing suitable optimization tools. This functional, at which $N$ means total number of calibrated specimens, $m$ expresses the rate of weighting of individual deviations, expresses total error of $\bar{\varepsilon}_f(\eta, \xi)$ in points $\left[\eta_{av_i}, \xi_{av_i}, \bar{\varepsilon}_{f_i}\right]$ corresponding with i-th specimen. More balanced deviation can be expected with growing value of $m$ ($m = 2$ corresponds with least squares method). Bai and Wierzbicki use modified target function $F^*_{av}$ in their work, Bai (2007. Individual deviations are weighted by fracture strain, Equation 23.

$$F^*_{av} = \frac{1}{N}\sum_{i=1}^{N}\frac{1}{\bar{\varepsilon}_{f_i}}\left| \bar{\varepsilon}_{f_i} - \bar{\varepsilon}_f\left(\eta_{av_i}, \xi_{av_i}\right)\right| \qquad 23$$

Optional application of least squares enabling employment of linear regression is quality of this approach. Some material models can be modified so that the linear regression can be used partially.

The second approach defines target as deviation of damage $\omega_i$ integrated up to fracture strain $\omega_{crit} = 1$ for i-th specimen averaged over all specimens, Equation 24.

$$F_\omega = \frac{1}{N}\sum_{i=1}^{N}\left| 1 - \omega_i \right|^m \;,\; \omega_i = \int_0^{\bar{\varepsilon}_{f_i}} \frac{d\bar{\varepsilon}_{pl_i}}{\varepsilon_f\left(\eta_i, \xi_i\right)} \qquad 24$$

This approach eliminates averaging in Equation 19 however calibration costs are higher in comparison with the first approach and moreover existence of global minimum uncertainty is higher in this case. For this reasons fine tuning of parameters that was found using averaging quantities is preferred application. This approach was used for example in Vaziri (2010).

## EXPERIMENT

Material calibration of ductile damage material model was carried out for two steels steel typically used in nuclear industry ferritic steel (used for pressure vessel) and austenitic steel (used for reactor pressure vessel internals). The portfolio of fifteen calibration specimen types for quasi-static loading was designed to calibrate fracture locus. Single specimens in space of stress triaxiality and Lode parameter are shown in Figure 2. It is based on averaged values of $\eta_{av}$ and $\xi_{av}$ at the instant of expected fracture.

The substantial subset of calibration portfolio is based on special specimen with double curvature (butterfly) that was described in Bai (2007). Essential advantage is possibility to cover wide range of stress triaxiality and normalized Lode angle with one specimen geometry only. Different stresses are caused by loading in different directions (tension: 0°, tension and shear: 30° - 90°, compression and shear: 100° - 130°). Another advantage is that damage initiation is always in the specimen centre. A special testing device was developed to perform calibration tests using uniaxial loading machine. It was shown during the testing verification phase that the experimental data was strongly influenced by friction in the guiding rods of the device. Therefore, simplified FE model of whole device was commonly used in numerical simulations of butterfly specimen. The friction coefficient was determined using trial and error

method to get correspondence with the experimental data. The disadvantage of this specimen type is shape complexity. The geometric inaccuracy may cause scattering between experimental data and FEM simulations. In basic position 0° three modifications of the butterfly with single thickness (T1), double thickness (T2) and triple thickness (T3) were measured without device. Examples of butterfly samples testing and simulation are shown in Figure 3.

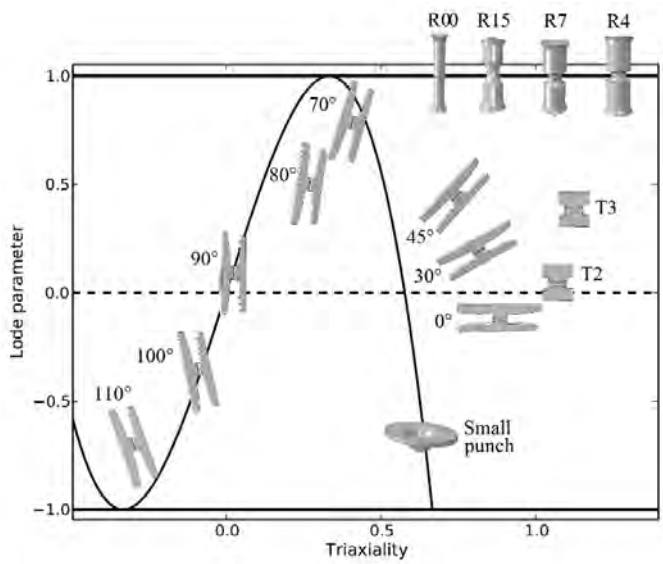


Figure 2. The portfolio of calibration specimens.

The second subset of calibration specimens consists of notched round bars with different notches radius (R∞, R15, R7 and R4). The specimen damage develops in conditions of constant value of Lode parameter $\xi = 1$. Each of these specimens was designed so that the fracture occurs first in the centre of the specimen.

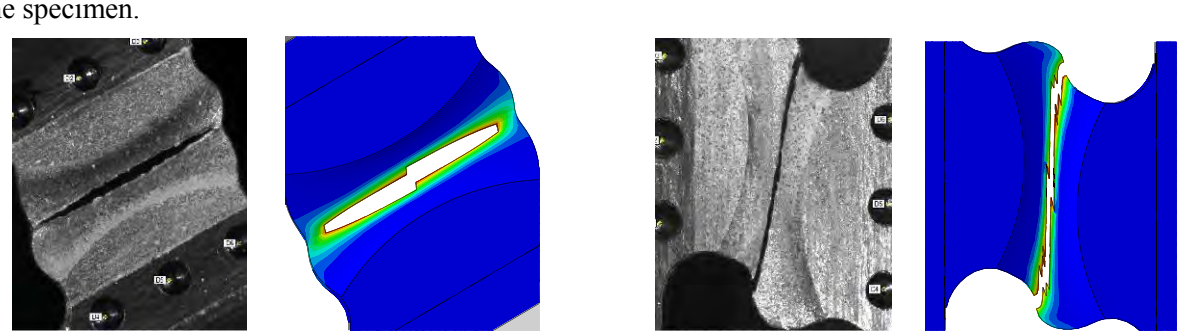

Figure 3. Comparison of butterfly specimens 30° and 90°. Numerical simulations and experiments.

The last calibration experiment is so called small punch test using miniature flat circular specimen through that the small steel ball is pushed. This experiment is used for verification of material properties of structures in operation from that small piece of material can be cut off without functionality loss. The specimen loading corresponds with biaxial tension. Disadvantage of this test is dependence on friction between ball and specimen.

## DAMAGE CALLIBRATION FOR FERRITIC STEEL

The calibration process was based on portfolio of fifteen different specimen types (Figure 2). The resultant fracture locus is shown in Figure 4. The figure introduces fracture strains of single specimens. Symbol associated with $i-\text{th}$ specimen is plotted at position $\left[\eta_{av_i}, \xi_{av_i}, \bar{\varepsilon}_{f_i}\right]$.

Fracture strain $\bar{\varepsilon}_f$ of this material exhibited independence on Lode parameter $\xi$. Therefore Johnson-Cook (the first term of Equation 12) and Rice-Tracey (Equation 13) material models are acceptable approximations for this kind of material. Figure 4 shows that Johnson-Cook fracture locus is negative for higher stress triaxiality ($\eta > 1.5$) due to negative parameter $d_1$. Therefore the fracture strain is supposed to be zero in that triaxiality range.

The results of FEM simulations for both used fracture locuses (Johnson-Cook and Rice-Tracey) are shown in consequent Figures 5 to 7. Response of Johnson-Cook material model is closer to experiments for most of specimens. It is possible to say that both models reach acceptable agreement with the experimental data.

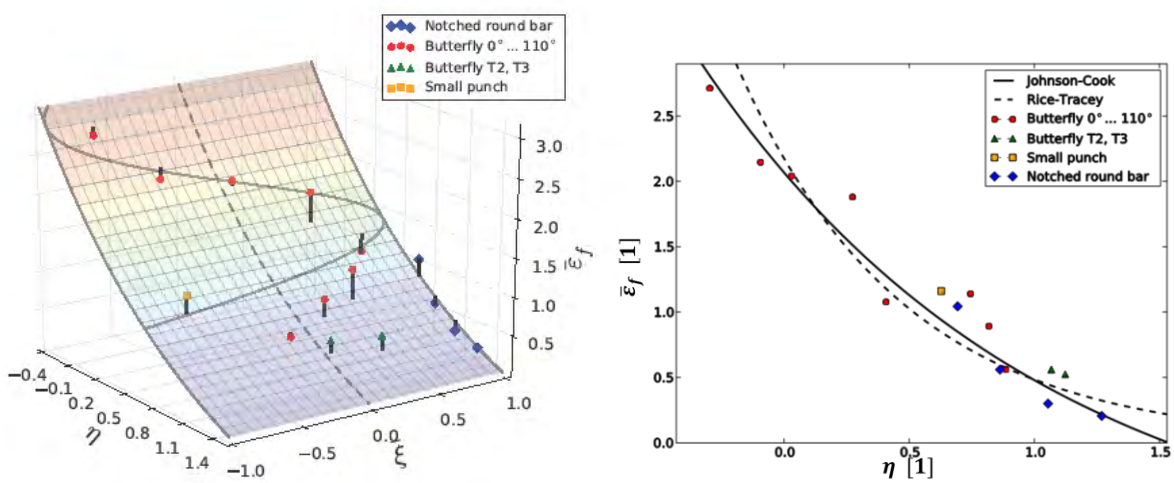


Figure 4. Resultant fracture locus - ferritic steel Johnson-Cook model (left), comparison of Johnson-Cook and Rice-Tracey models (right)

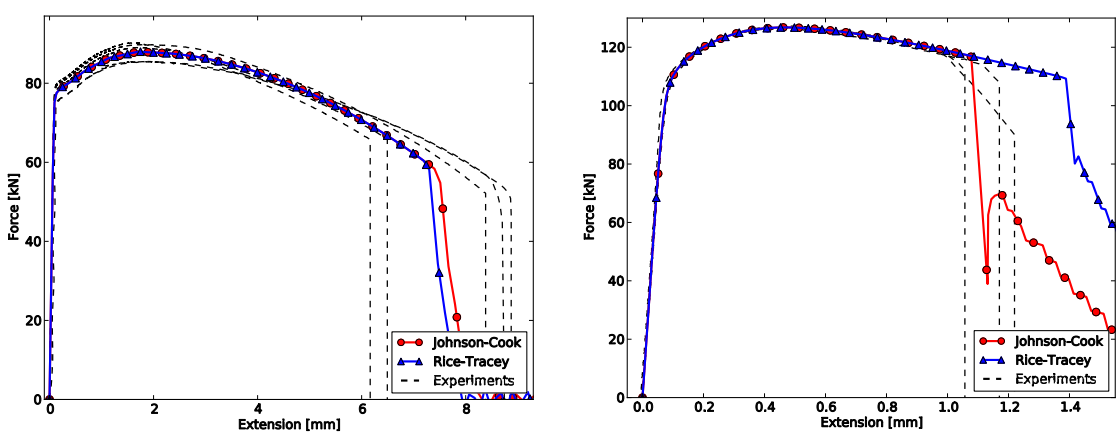


Figure 5. The load - extension response from FE analysis in comparison to experiments. Specimens smooth round bar R∞(left), notched round bar R4 (right).

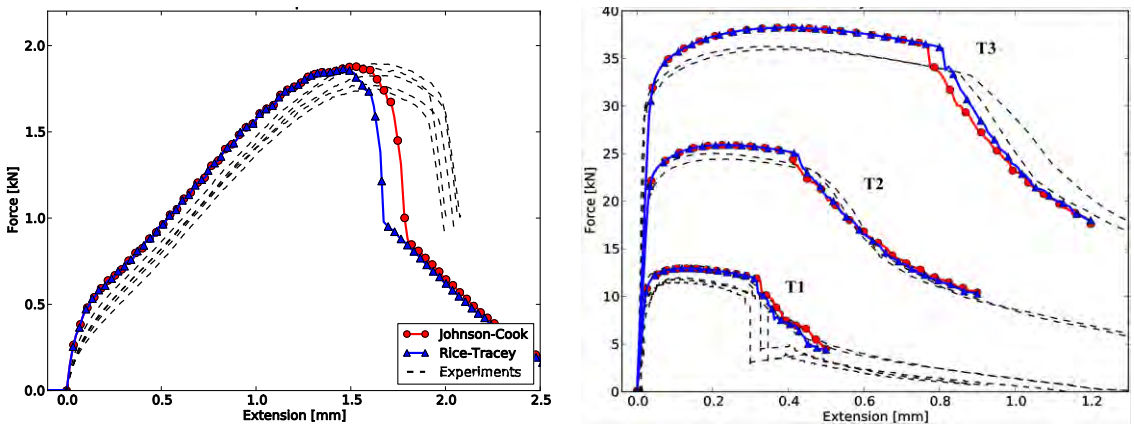


Figure 6. The load - extension response from FE analysis in comparison to experiments small punch test specimen (left), Butterfly specimen 0° with different specimen thickness, (right).

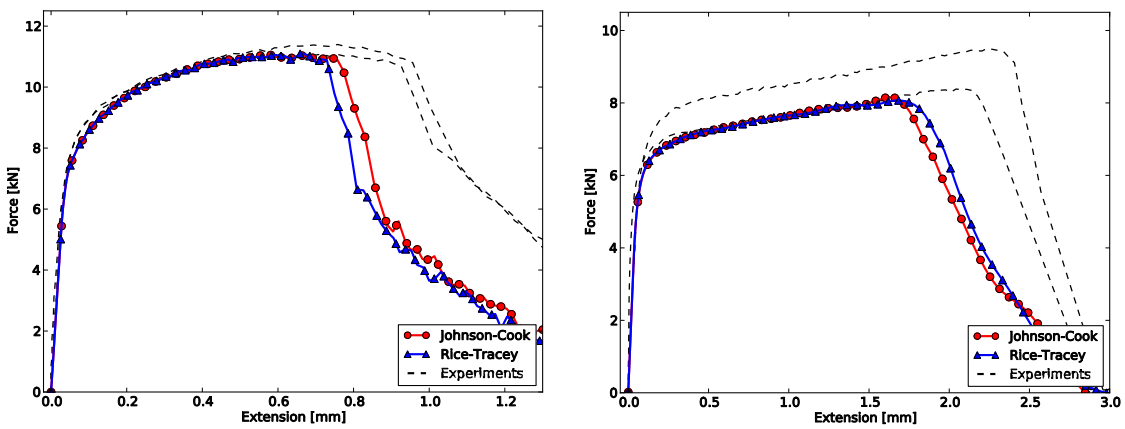


Figure 7. The load - extension response from FE analysis in comparison to experiments. Specimens butterfly 45° (left), butterfly 90° (right).

## DAMAGE CALLIBRATION FOR AUSTENITIC STEEL

In the case of the austenitic steel investigation the Bai-Wierzbicki material model was calibrated using modified target functional Equation 22. The calibration process was based on a portfolio of fifteen different specimen types (Figure 2). The resultant fracture locus is shown in Figure 8. Short bars with symbols introduce the fracture strains of individual specimens. The symbol associated with the specimen is plotted at position. The dependence of the quadratic Lode angle (3) in the Bai-Wierzbicki model is not an optimal approximation in this case. For this reason, a modification of the model was tested. The quadratic form (3) was replaced by a fourth order polynomial function in the form of Equation 25

$$\bar{\varepsilon}_f\left(\eta,\bar{\theta}\right) = A_1(\eta)\bar{\theta}^4 + A_2(\eta)\bar{\theta} + A_3(\eta) \qquad 25$$

The resultant modified fracture locus plotted in Figure 8 is slightly closer to the experimental points. In the theoretical part of this paper, we described an element deletion procedure based on gradual degradation D. The degradation rate is controlled by Hillerborg fracture energy $G_f$ . The influence of the fracture energy on the simulated loading curve for butterfly 0° and for small punch specimens is demonstrated in Figure 10. Fracture energy values close to zero ($G_f = 0{,}01\text{Nmm}^{-1}$) loose toughness faster than in the experimental tests. This effect manifests itself namely in the case of butterfly specimens. The fracture energy was changed to a value of $G_f = 20\text{Nmm}^{-1}$ to make the simulations closer to the experiments. However, mesh density dependence is introduced into the simulations by this step. As the

meshes of all specimens except the small punch specimen are of uniform density with the same edge length 0,2mm in the domain of interest, this value is correct for all except the small punch specimen, which uses a four times denser mesh. For this reason, the fracture energy value for the small punch specimen was recalculated according to Equation 19.

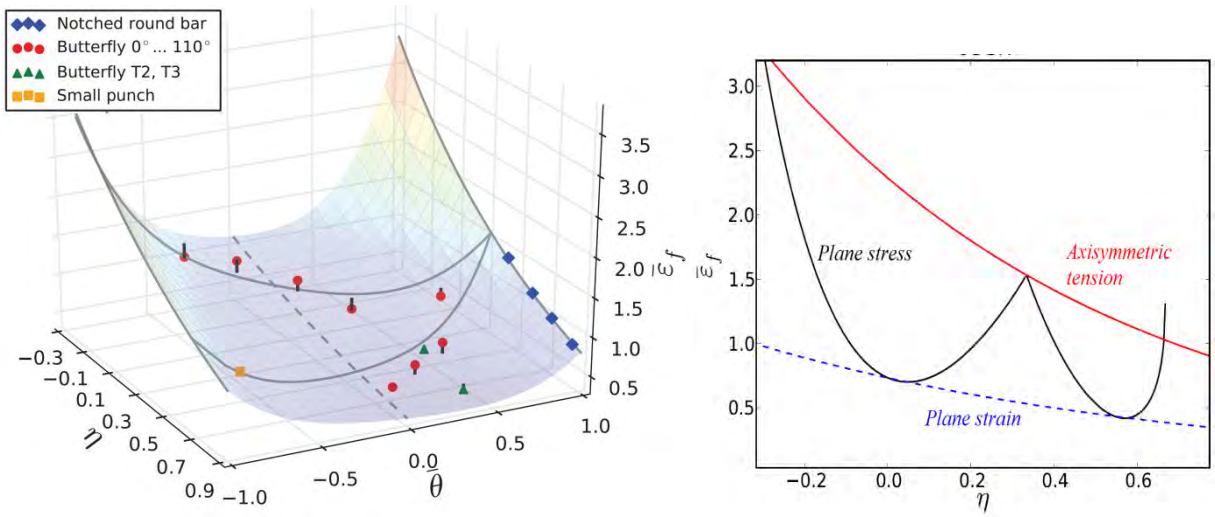


Figure 8. Resultant Bai-Wierzbicki fracture locus – austenitic steel

The results of the FE simulations for both fracture loci used here (Bai-Wierzbicki and Modified Bai-Wierzbicki) are shown in Figures. 9 - 11. For most of the specimens, the response of the modified Bai-Wierzbicki material model is closer to the experiments than the original response. An exception is the notched round bar R4, Figure 9. The fracture of this specimen is initiated earlier in the modified than in the original Bai-Wierzbicki model. Simulation with modified Bai-Wierzbicki material model exhibits misplaced fracture initiation in the notch instead of in the axis of the specimen. Metallographic observation of specimens that were damaged but not fractured proved that cavity growth begins from the center of specimen. This is in agreement with the material model based on the original Bai-Wierzbicki fracture locus. It can be said that both models achieve acceptable agreement with the experimental data. Significant differences occurred in the butterfly T3, butterfly 90° and butterfly 100° specimens.

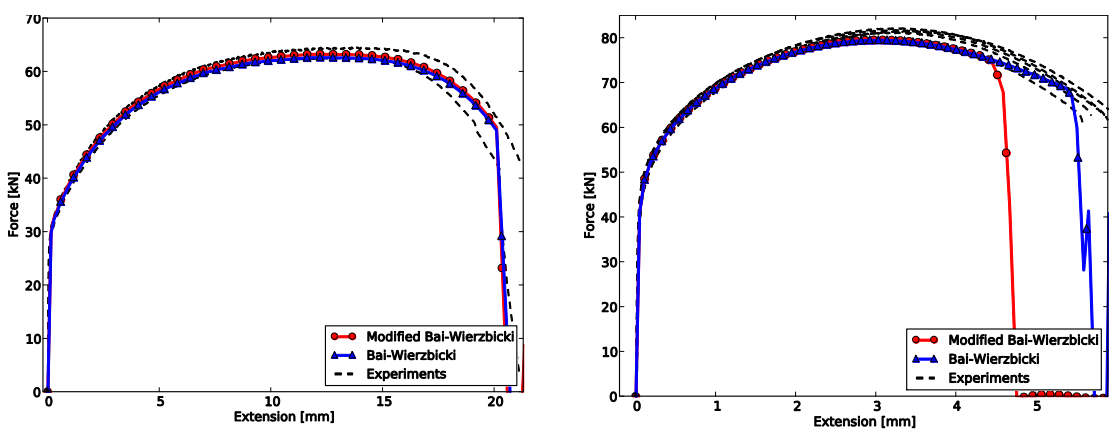


Figure 9. The load - extension response from FE analysis in comparison to experiments. Specimens smooth round bar R∞(left), notched round bar R4 (right).

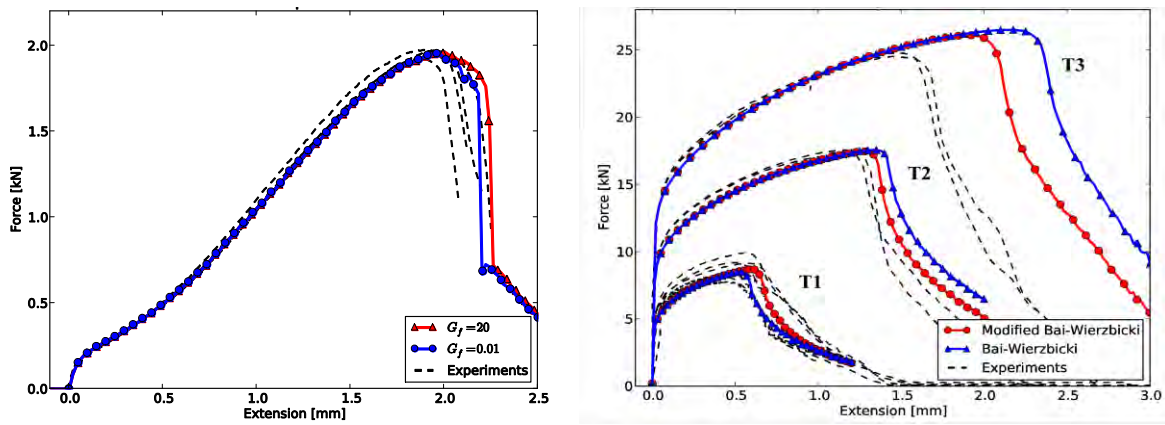


Figure 10. The load - extension response from FE analysis in comparison to experiments small punch test specimen (left), Butterfly specimen 0° with different specimen thickness, (right).

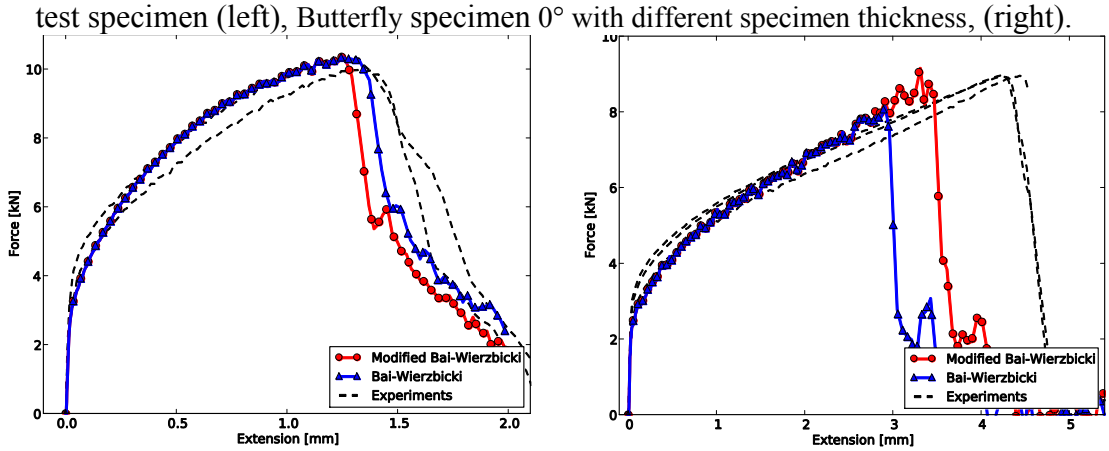


Figure 11. The load - extension response from FE analysis in comparison to experiments. Specimens butterfly 45° (left), butterfly 90° (right).

## THE SPECIMENS WITH HIGH STRAIN CONCENTRATION

Calibration of material model that was performed using fifteen different specimens has proved ductile fracture of tested material dependency on stress triaxiality. Calibrated material model was tested on a few other specimen types with high stress concentration. Specimens typically used in fracture mechanics – notched CT samples - without pre-crack were employed.

The comparison of experimental response of the specimens with FEM simulations for ferritic steel using Johnson-Cook and Rice-Tracey material model is presented in the Figure 12. Ductile fracture model failed for CT when using Johnson-Cook ductile fracture model, but the result of Rice-Tracey model is well acceptable.

A comparison of the experimental response of the specimens with the FEM simulations for the austenitic steel using the Bai-Wierzbicki material model and the Modified Bai-Wierzbicki material model is presented in Figure 12. FEM simulation of CT gives wrong results in comparison with the experimental measurements at extensions above 3,5mm. There was no fracture during the experimental loading. However, the FEM simulations exhibit rapid damage and the crack propagation through the specimen.

The material model discussed in this paper was not able to provide a successful description of the localized strain concentration for the austenitic steel. The nonlinear damage accumulation was tested in the calibration process, but the local strain concentration was not successfully resolved. Uncoupled ductile damage models based on a fracture locus that is dependent only on stress triaxiality and the normalized Lode angle seem to be unable provide us with correct fracture predictions in the case of high strain concentration of materials with very high ductility.

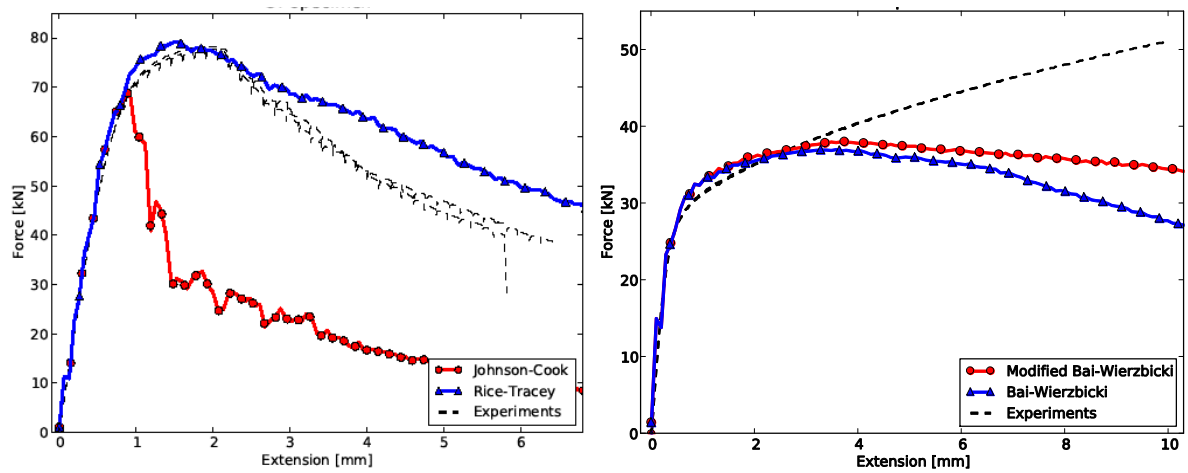


Figure 12. Comparison of simulation with experiment for CT. Ferritic steel (left), austenitic steel (right)

## CONCLUSION

Ductile damage parameters determination for two RPV steels, austenitic and ferritic, was performed here with the use of Johnson-Cook, Rice Tracey and Bai-Wierzbicki models. The obtained material models were subsequently applied to simulation of notched CT fracture toughness specimens and the results were compared with the experimentally obtained results in order to assess materials models applicability.

As a first step of the investigation there were proposed samples geometries with various states of stress triaxialities and values of Lode parameter. These various conditions were necessary in order to describe a broad range of plastic behavior. Round samples with notches of radius 4, 7 and 15 mm and smooth ones were tested together with butterfly type of samples tested at 8 different angles together with small punch tests. Altogether 15 samples configurations sets were used for each material for ductile damage parameters determination.

The experimental results were used as an input data for ductile damage parameters identification. Plasticity and ductile damage parameters identification was done with the use of open optimization scripts in Python, that can minimize the function by change of the variables. A simplex based algorithm was used for local optimization. The optimization was done on the basis of minimization of the area between measured and calculated curves. The optimization was done for complete set of the samples investigated simultaneously. The parameters identified were subsequently used for FEM simulation of notched three point bend sample testing. The obtained records from experiment and FEM simulation exhibited very good result for both materials investigated. In the case of the ferritic steel it was found that the material is not sensitive to Lode parameter, while the austenitic steel shown strong sensitivity to this parameter.

The final part of the paper was dealing with assessment of the applicability of the the models considered for calculation of samples with high local strain concentrations such as fracture mechanics CT samples. Very good agreement was found for ferritic steel between the simulation with the use of Rice-Tracey model, while Johnson-Cook model exhibited premature fracture of the sample. In the case of the austenitic steel there was good agreement between measured and simulated results up to extension of about 3,5mm. From that point, the measured and simulated curves strongly differ and the simulation predicts rapid fracture, while the experiments does not not show any crack growth within considered extensions range.

The austenitic steel exhibits large ductility and uncoupled ductile damage models based on the fracture locus seem not to be applicable to cope with extremely large local plastic strains.

Coupled ductile fracture material models Wierzbicki (2005), gradient models, stochastic models Krieg (2003) may deal effectively with high strain concentrations.

Further investigations will be carried out on material exhibiting stable crack growth at considered conditions. Also investigation of the materials ductile behavior will be carried out at increased temperature and dynamic loading conditions. A challenge is procedures development for ductile damage parameters identification based on measurements of miniature samples available in cases e.g. when remnant service evaluation of in service structures is established.

## ACKNOWLEDGEMENT

This work was done within the work on the project "TA02010992 - Development and validation of the welding and heat treatment numerical simulation including simplify numerical lifetime prediction of welded joints for new trend materials which are using in energy sector, airplane and space industry" sponsored by Technology Agency of The Czech Republic.

## REFERENCES

Bai, Y., Wierzbicki, T. (2010). "Application of extended Mohr–Coulomb criterion to ductile fracture", Int J Fract 161, 1–20.

Bai, Y., Wierzbicki, T. (2008). "A new model of metal plasticity and fracturewith pressure and Lode dependence", International Journal of Plasticity 24, 1071–1096.

Wierzbicki ,T. et al., (2005). "Calibration and evaluation of seven fracture models", International Journal of Mechanical Sciences 47, 719–743.

Bao, Y., Wierzbicki, T. (2004). "A Comparative Study on Various Ductile Crack Formation Criteria", Transactions of the ASME, Vol. 126, 314-324.

Li, Y., Wierzbicki, T. (2009). "Mesh-size Effect Study of Ductile Fracture by Non-local Approach", Proceedings of the SEM Annual Conference June 1-4, Albuquerque New Mexico USA.

Rice JR, Tracey DM. (1969). "On the ductile enlargement of voids in triaxial stress fields". Journal of the Mechanics and Physics of Solids;17:201–17.

Wierzbicki T., Xue L.(2005), "On the effect of the third invariant of the stress deviator on ductile fracture", Technical report, Impact and Crashworthiness Laboratory, Massachusetts Institute of Technology, Cambridge.

Bai Y, Teng X, Wierzbicki T. (2007). "Derivation and application of stress triaxiality formula for plane strain fracture testing". ASME conference, Austin, Texas.

Vaziri M.R., Salimi M., Mashayekhi M. (2010). "A new calibration method for ductile fracture models as chip separation criteria in machining", Simulation Modelling Practice and Theory 18, 1286–1296.

Wierzbicki T, Xue L. (2005). "On the effect of the third invariant of the stress deviator on ductile fracture". Tech. Rep.; Impact and Crashworthiness Laboratory, Massachusetts Institute of Technology, Cambridge, MA; 2005.

Krieg R, Seidenfuss M.(2003) "Limit strains for severe accident conditions final report of the eu-project lissac", contract no. fiks-ct1999-00012. Wissenschaftliche Berichte FZKA 2003;6854. Eng; URL http://www.refdoc.fr/Detailnotice?idarticle=9048938.

## COPYRIGHT TRANSFER AGREEMENT

The below text in italic is for your information and agreement prior to submittal of the paper.

*The author(s) warrants that the submitted manuscript is the original work of the author(s) and has never been published in its present form.*

*The Lead Author, with the consent of all other authors, by submitting the manuscript for publication in SMiRT-22 transactions, hereby transfers copyright interest in the submitted manuscript to IASMiRT subject to the following.*

- *The Lead Author and all coauthors retain the right to revise, adapt, prepare derivative/ expanded works, present orally, or distribute the work.*
- *In all instances where the work is prepared as a "work made for hire" for an employer, the employer(s) of the author(s) retain(s) the right to revise, adapt, prepare derivative/expanded works, publish, reprint, reproduce, and distribute the work provided that such use is for the promotion of its business enterprise and does not imply the endorsement of IASMiRT.*
- *It is recognized that an author who is a U.S. Government employee and who has participated in the submitted work does not own copyright in it.*

*Note: If the manuscript is not accepted by IASMiRT or is withdrawn prior to acceptance by IASMiRT, this copyright transfer will be null and void.*